Cell mechanics in biomedical cavitation

Kuo-Kang Liu [a*], Kawa Manmi [b] and Qianxi Wang [b]
[a]School of Engineering, University of Warwick, CV4 7AL, UK
[b]School of Mathematics, University of Birmingham, B15 2TY, UK

Abstract

Studies on the deformation behaviours of cellular entities, such as coated microbubbles and liposomes subject to a cavitation flow, become increasingly important for the advancement of ultrasonic imaging and drug delivery. Numerical simulations for bubble dynamics of ultrasound contrast agents (UCAs) based on the boundary integral method are presented in this work. The effects of the encapsulating shell are estimated by adapting Hoff's model used for thin-shell contrast agents. The viscosity effects are estimated by including the normal viscous stress in the boundary condition. In parallel, mechanical models of cell membranes and liposomes as well as state-of-the-art techniques for quantitative measurement of viscoelasticity for a single cell or coated microbubbles are reviewed. The future developments regarding modelling and measurement of the material properties of the cellular entities for the cutting-edge biomedical applications are also discussed.

Keywords: Ultrasonic Cavitation, Membrane Mechanics, Microbubble Dynamics, Single-cell Mechanics, Boundary Integral Method (BIM)

KKL and QXW contributed equally to this study
*e-mail: i.k.liu@warwick.ac.uk

1. Introduction

It becomes increasingly prevalent~~prevailing~~ for cavitation to be applied to biomedicine including ultrasound contrast agents (UCAs), drug delivery (Coussios & Roy 2008), sonoporation (Yu & Xu 2014**)**, and cell separation (Patent US20120164113 A1). A better understanding of the complex interplay between a cavitational flow and a cell or cell-like membrane is of paramount importance to the fundamental optimization of these applications. An interdisciplinary approach combining cell mechanics with bubble dynamics can be highly desirable to elucidate the deformation behaviors of cellular entities subject to cavitation flow and to enhance drug delivery via the coated micro-bubbles (Tsutsui *et al* 2004). These developments will fundamentally advance our knowledge of targeted drug delivery and sonoporation. They will also have important applications in ultrasound diagnostics, such as analysing potential bio-effects of ultrasound-activated-microbubbles on micro-vessels. Moreover,

Typical UCAs are micron-sized (typically between 0.5 and 10 μm in diameter) gas bubbles stabilized by biologically inert coatings such as lipid, protein and polymer (Sirsi & Borden, 2010). A recent~~comprehensive~~ review~~description~~ introduces compressively ~~of the~~ state-of-the-art ~~diverse~~ ~~microbubble generation~~technique~~ method~~s to generate both the coated and un-coated microbubble and a theoretical model to describe the physics of the bubble formations ~~is reviewed by~~ (Rodr´ıguez-Rodr´ıguez et al. 2015). ~~-~~Their paper also reports several modern techniques to produce UCAs which are coated with phospholipid shell ~~membrane~~ or surfactant membrane~~shell~~, and concludes that microfluidics is a promising approach to control precisely the sizes and coating properties of UCAs in their production~~formation~~s.

UCAs are rapidly evolving from the diagnostic modality into a therapeutic tool (Coussions & Roy, 2008). One important potential application is to use UCAs to deliver a drug/gene for ultrasound therapy, e.g., cancer treatment (Ibsen *et al* 2013). Upon arriving at a targeted site, the microbubbles are activated by ultrasound leading to violent collapse. This releases the drug/gene cargo and also causes cell membranes nearby to become temporarily leaky, a phenomenon known as sonoporation (Carson *et al*., 2011; Kaul, 2004). The mechanism aids the gene/drug to enter the target cells via diffusion and also convection if microjets arise (Shen *et al*., 2008; Marmottant & Hilgenfeldt 2003; Ferrara *et al.*, 2007).

Targeted drug delivery improves disease treatment efficacy and safety, as well as patient convenience and compliance. It is of particular interest for pharmaceutical agents that yield detrimental side effects. It has been generating worldwide interest in the communities of both

scientists and clinical researchers (Coussions & Roy, 2008). Detailed experimental studies have revealed considerable evidence of the leaking of a transported drug from the coated bubbles. It has been established by numerous groups, that the localized cellular uptake of drugs/genes is significantly increased when microbubbles are present (Coussions & Roy, 2008).

On the theoretical front, c~~C~~oated bubble dynamics is an extension of traditional bubble dynamics. Most studies on the topic were based on spherical bubble theory, the Rayleigh–Plesset equation incorporated with linear and nonlinear cellular membrane models (Postema *et al*, 2004), and the shape stability of a nearly spherical bubble (Liu, *et al.*, 2012). However, nonspherical coated bubbles frequently present in medical applications, such as: (i) the onset of breaking of the bubble coating in releasing drugs is directly linked to the loss of spherical symmetry (Coussions & Roy, 2008), (ii) the sonoproation is associated with a bubble interacting with a cell nearby (Coussions & Roy, 2008). Chen et al. (2011) observed that coated ultrasound bubbles in micro-blood-vessels of rat mesentery are often associated with non-spherical deformation and liquid jetting and the study shows there is a need to develop new theoretical models for describing non-spherical deformation of bubbles (see Fig. 1).

Lipid bilayer forming the major constituent of plasma membrane plays a crucial role in sustaining the integrity and functions of biological cells. Liposome is an artificial cellular entity (a few micrometers in diameter) where a liquid drop or gas is closed by a lipid bilayer membrane (~~ca~~ about 10 nm in thickness) and is often used as model cell in biomechanical study. Liposome has long been used as drug delivery vehicles by encapsulating drugs within the bilayer membrane since it exhibits excellent biocompatibility such as longer life span in blood circulation, low toxicity and easily untaken by targeted tissue (Paul *et al*., 2014). Recently ultrasonic cavitation has been applied to trigger or induce drug release from liposome (Schroeder *et al*., 2009) (see Fig. 2~~1~~). The mechanical characterization of a single liposome attracts increasing interests in the scientific community, for instance, analysis of the deformation of lipid coated microbubble or echogenic liposome for both drug delivery and sonoporation (Sundaram *et al*., 2003).

Theoretical models integrating bubble dynamic with mechanics of cell membrane or coated membrane are desirable for design of the next generation of ultrasonic contrast agents and drug delivery systems. In Section 2, numerical simulations for dynamics UCAs based on the boundary integral method are presented based on a simple model for the coating shell of microbubbles. We also review mechanical models of bubble coating and liposome in Section

3 and the state-of-the-art techniques for quantitative measurement of viscoelasticity of a single cell or coated microbubble in Section 4.

2. Dynamics of coated-micro-bubbles based on Hoff's model

2.1 Computational bubble dynamics

The boundary integral method (BIM) based on the potential flow theory is grid-free in the flow domain and has been widely used in bubble boundary interactions for axisymmetric cases (Guerri *et al*., 1981; Blake *et al*., 1986, 1987; Brujan *et al*., 2002; Szeri *et al*., 2003, Wang et al., 1996a, b, 2005; Lind & Phillips, 2012; Curtiss *et al*., 2013) and for three dimensional configurations (Wang, 1998, 2004; Klaseboer *et al*., 2005, Jayaprakash et al. 2012). Recently Wang et al. (Wang & Blake, 2010, 2011; Wang, 2013, 2014) developed the BIM for bubble dynamics in a compressible liquid.

Bubble dynamics have been simulated using domain approaches, such as, the high-order accurate shock- and interface-capturing scheme (Johnsen & Colonius, 2009), orthogonal boundary-fitted grids for axisymmetric bubbles (Yang& Prosperetti, 2008), the free-Lagrange method (Turangan *et al*., 2008), the arbitrary Lagrangian Eulerian method (Yue *et al*., 2007) and front tracking method coupled with SIMPLE algorithm (Hua & Lou, 2007). Direct simulation for multiple oscillations of acoustic bubble is highly computational demanding. It is a multi-scale problem when the compressible effects of the liquid are not negligible, since the wavelength is much larger than the bubble radius. It involves a large computational domain for describing the propagation of the acoustic wave, and a very long time interval. Hsiao & Chahine (2013) recently modeled the bubble coating using a layer of a Newtonian viscous fluid, to study the mechanism of bubble break-up during non-spherical deformations resulting from the presence of a nearby rigid boundary. The effects of the shell thickness and the bubble standoff distance from the solid wall on the bubble break-up were studied parametrically.

Consider the dynamics of UCAs near an infinite rigid plane wall subject to ultrasound, as shown in figure 3. We assume that the fluid surrounding the bubble is incompressible and the flow is irrotational. The fluid velocity $\boldsymbol{v}$ thus has a potential φ, $\boldsymbol{v} = \nabla\varphi$, which satisfies Laplace's equation, $\nabla^2\varphi = 0$. Using Green's second identity the potential φ can be represented as a surface integral over the bubble surface S as follows:

$$c(\boldsymbol{r})\varphi(\boldsymbol{r}) = \int_S \left(\frac{\partial \varphi(\boldsymbol{q})}{\partial n} G(\boldsymbol{r},\boldsymbol{q}) - \varphi(\boldsymbol{q}) \frac{\partial G(\boldsymbol{r},\boldsymbol{q})}{\partial n} \right) dS(\boldsymbol{q}), \tag{2.1}$$

where $\boldsymbol{r}$ is the field point and $\boldsymbol{q}$ is the source point, $c(\boldsymbol{r})$ is the solid angle and $\boldsymbol{n}$ is the unit outward normal of the bubble surface S directed from liquid to gas. To satisfy the impermeable boundary condition on the wall, the Green function is given as follows, $G(\boldsymbol{r},\boldsymbol{q}) = |\boldsymbol{r}-\boldsymbol{q}|^{-1} + |\boldsymbol{r}-\boldsymbol{q}'|^{-1}$, where $\boldsymbol{q}'$ is the image of $\boldsymbol{q}$ reflected to the wall.

The kinematic boundary condition on the bubble surface is

$$\frac{d\boldsymbol{r}}{dt} = \nabla\varphi. \tag{2.2}$$

The dynamics boundary condition on the bubble surface is

$$\frac{d\varphi}{dt} = \frac{1}{2}|\nabla\varphi|^2 + \frac{1}{\rho}\left(-p_g + p_\infty(x,t) + \frac{2\sigma}{R_c} + \Delta T \right), \tag{2.3}$$

where ρ is the liquid density and σ is the surface tension coefficient.The first term p_g in the right bracket is the gas pressure inside the UCA. Since we consider the rapidly collapsing bubbles, p_g is assumed following the adiabatic law $p_g = p_{g0}(V_0/V)^{\alpha}$. Here p_{g0} is the initial gas pressure inside the UCA, V and V_0 are the instantaneous and initial bubble volumes, respectively. α is the ratio of specific heats of the interior gas. Unless otherwise noted, we set α = 1.67 (argon) for the simulations presented here. The second term $p_\infty(x,t)$ is the far-field pressure, $p_\infty(x,t) = p_0 + p_a \sin(kx - \omega t)$, where p_0 is the hydrostatic pressure, x is the coordinate along the direction of the wave, t is time, and p_a, k and ω are the pressure amplitude, wavenumber and angular frequency of the acoustic wave, respectively.

The third term is associated with the surface tension effect, where σ is the surface tension and R_c is the curvature radius of the bubble surface. The fourth term is the radial pressure difference $\Delta T = T_2 - T_1$ (see Fig. 3), which is approximated by adapting Hoff's model (Hoff, 2001) for the thin-shell of spherical contrast agents, by replacing the bubble radius with the local curvature radius R_c as follows:

$$\Delta T = 12\frac{d_s}{R_0^2}\left(\frac{R_0}{R_c}\right)^4 \left[G_s(R_c - R_0) + \mu_s \dot{R}_c \right], \tag{2.4}$$

where R_0 is the initial bubble radii, d_s is the shell thickness, and G_s and μ_s are the shear modulus and shear viscosity of the shell, respectively. The overdot denotes differentiation with respect to time.

We choose the reference length R_0 (initial radius of the bubble) and the reference pressure p_0 to introduce the following dimensionless quantities denoted by an asterisk (*),

$$p_{a^*} = \frac{p_a}{p_0}, \qquad \sigma_* = \frac{\sigma}{R_0 p_0}, \tag{2.5}$$

$$\varepsilon = \frac{p_{g0} + 2\sigma/R_0}{p_0}. \tag{2.6}$$

Following convention, the standoff distance is nondimensionalized with respect to the maximum equivalent bubble radius,

$$\gamma = \frac{s}{R_{\max}}, \tag{2.7}$$

where s is the distance between the wall and the bubble centre at inception (see figure 3), and $R_{\max}$ is the maximum radius a bubble initially in equilibrium would attain in an infinite ambient fluid subject to the imposed ultrasound.

We argue this simplified model can be used to approximate the essential effects of the coating for the following reasons. An encapsulated bubble is usually approximately spherical during most of its lifetime except for a short period during the end of collapse when the bubble becomes nonspherical. This model thus provides a good estimation for the influence of the shell on the bubble, the asymmetric flow and pressure fields prior to jet development. When liquid jetting starts, the large asymmetric momentum of the liquid flow and high pressure of the bubble gas are dominant effects; the elastic and viscous effects of the thin coating should be secondary effects.

2.3 Numerical results

To validate this model for the restricted case of spherical oscillation of a coated bubble, the results were compared to the modified Rayleigh-Plesset equation used by Hoff (2001) that accounts for the elastic and viscous effects of the shell. Using the present notation, this equation is given by

$$\rho\left(R\ddot{R} + \tfrac{3}{2}\dot{R}\right) = p_{g0}\left(\frac{R_0}{R}\right)^{3\alpha} - p_\infty(x,t) - 12\mu_s \frac{d_s R_0^2}{R^3}\frac{\dot{R}}{R} - 12G_s \frac{d_s R_0^2}{R^3}\left(1 - \frac{R_0}{R}\right). \tag{2.8}$$

Note that the terms for the liquid viscosity and time derivative of the liquid pressure are neglected in the above equation, as we assume an inviscid and incompressible liquid.

Figure 4 shows comparisons of the bubble radius time history for a coated and uncoated bubble as determined from the 3D BIM model and modified Rayleigh-Plesset (RP). The BIM model agrees well with the modified RP for several cycles of oscillation for both of the coated and uncoated bubbles oscillating spherically subject to ultrasound.

We study microbubble dynamics near a rigid wall subject to ultrasound propagating parallel to the wall. To study the effects of the standoff distance of the bubble from the wall, we consider three cases (figure 5-7) at γ = 1.0, 2.0 and 3.0, respectively, for p_{a^*} = 2.0, with the remaining parameters the same as in figure 5.

The figure 5 shows the typical bubble shapes for the case at γ = 3.0 at various stages during the expansion phase (5a-b) and collapse phase (5b-d). The bubble remains approximately spherical during the expansion and collapse phases except for a high-speed liquid jet that develops rapidly towards the end of the collapse phase. The bubble is subject to the primary Bjerknes force due to the acoustic wave and the secondary Bjerknes force due to the wall. The primary Bjerknes force is along the wave direction and the secondary Bjerknes force is perpendicular to the wall. The jet is along the bisector of the two forces (figures 5d), which suggest the two forces are comparable in this case as in the uncoated bubble (Wang & Manmi 2014).

For the case at γ = 2.0, the bubble again remains spherical for most of its lifetime and a high-speed liquid jet develops at the last stage of collapse, as shown in figure 6. The jet is wider and its direction rotates pointing more to the wall in comparison to the case at γ = 3.0, since the second Bjerknes force due to the wall is stronger in this case.

The bubble shapes for γ = 1.0 at typical stages of deformation are shown in figure 7. The bubble surface proximal to the wall is slightly flattened due to the wall during the last stage of expansion (figure 7b). The bubble collapses nonspherically and a large liquid jet develops on the distal side of the bubble directed towards the wall. The jet development time is only 0.5% of the bubble lifetime for the cases γ = 3.0 and 2.0, but is 1.5% for the case γ = 1.0.

3. Dynamics of the coating membrane

The membrane of a coating bubble or an encapsulated liposome is usually very thin of *O*(1-10) nm and soft, made of a polymer shell or liposome (an artificially-prepared cellular entity). It is assumed to be infinitely thin and isotropic in their planes. The elasticity of the membrane can be described by the Mooney-Rivlin law (Tsigklifis & Pelekasisa, 2013)

$$\tau_i = \frac{\lambda_i}{\lambda_1\lambda_2}\frac{\partial W}{\partial \lambda_i},\ i=1,\ 2, \quad W = \frac{G_s}{2}\left(\lambda_1^2+\lambda_2^2+\frac{1}{\lambda_1^2\lambda_2^2}-3\right), \tag{3.1}$$

where λ_1 and λ_2 are the principle stretches, τ_1 and τ_2 are the corresponding in-plane tensions, and G_s is the surface modulus of elasticity. As cellular deformations, coated micro-bubbles or liposomes subject to ultrasound exposure normally exhibit visco-elastic behaviours in their deformations and hence a more compressive model which includes the viscoelasicity has been introduced recently (Doinikov *et al.*, 2009). The following term should be added to Eq. (3.1) for producing the constitutive equations of a viscoelastic material

$$\tau_i^{\mathrm{v}} = 2\mu_s\lambda_i\frac{\partial \lambda_s}{\partial t},\ i=1,\ 2, \tag{3.2}$$

μ_s is the surface modulus of viscosity and τ_i^{v} is the tensions contributed by viscosity. Alternately the membrane of encapsulated liposome can be portrayed by cell mechanical models which are described in details in the following section.

The transverse shear tension $\boldsymbol{q}$ is given in terms of the bending moment $\boldsymbol{m}$ expressed in a similar form to that of the in-plane stress (Chen et al., 2011). The membrane stress is then given as

$$\boldsymbol{F}^m = -(\boldsymbol{I}-\boldsymbol{nn})\cdot(\boldsymbol{\tau}+\boldsymbol{qn}). \tag{3.3}$$

The governing equations for the coating

$$F_n = -p_b + \frac{\kappa}{W_e} + F_n^m, \qquad F_\tau = F_\tau^m, \tag{3.4}$$

where p_b is the pressure of the bubble and κ the curvature of the surface. W_e is the Weber number $W_e = R_0 p_\infty/\sigma$. We assume that the shear stress of the gas on the coating is negligible, as viscosity of gases is much smaller than that of liquids.

The BIM model described in § 2 can be developed to model the interaction of coated bubble dynamics and coating membrane dynamics. At each step the stress distributions F_n and F_τ are provided from the fluid modeling, and the membrane modeling will then provide the velocity distribution of the coating or liposome membrane, which are subsequently used as the inputs for the fluid modeling.

4. Cell mechanics models

Deformation of a biological cell is a complex interplay between the interfacial, mechanical and viscoelastic components such as filaments, extra-cellular matrix, and membranous organelles, their distinct geometry and characteristics, the microstructure within the cell, and

the concerted deformation of each component in response to external load. To determine these parameters, a comprehensive biomechanical model is necessary to extract the information from measurements such as Poisson's ratio, Young's modulus, internal pressure, bursting strength, and viscoelasticity etc. The model is also expected to relate these intrinsic materials properties to the macroscopic manifestation of the overall cellular deformation behaviors. Since most biomimetic/biological cells comprise of non-linear, inhomogeneous, anisotropic, and viscoelastic materials, their constitutive laws and the embedded stress-strain relationships cannot be adequately described by conventional linear elasticity. Large deformation theory, in conjunction with the non-linear Moony-Rivlin constitutive equations, is adopted for polymeric vesicle or microbubble shown as equation (3.1) (Barthes-Biesel, 2003), while liposome mechanical model is best suit for describing specifically deformation of liposome or lipid-coated bubble in various situations (Li et al 2006). The existing models are apparently inadequate to portray an actual biological cell in full details, except certain specific simple structures such as the mature erythrocytes which possess neither organelles nor nuclei within the cell membrane. The latest drive is to develop appropriate theoretical models which include the large deformation formulation, non-linear elasticity and viscosity. These higher-order models are obviously more comprehensive than most of the previously reported studies which belong to first-order analyses.

4.1 Elastic shell model

Mechanical models for describing the mechanics of liposome or coated bubble have been long endeavored and resulted in two major categories: bending stiffness dominating (Waugh et al., 1992) and extensional modulus dominating (Skalak et al., 1973). The former models a cell as a thin spherical elastic membrane filled with liquid or air, similar to a balloon, while latter describes cell membrane as a rigid thick shell. Based on these developments, a model which combines both of the extensional and bending effects has latter been developed for analyzing liposome deformation induced by pressure change (Pamplona and Calladine, 1993). It is worthy of pointing out that liposome possesses surface and mechanical behaviors similar to biological cells and hence several cell mechanical models are developed based on the study of liposome mechanics (Parker and Winlove, 1999, Foo et al 2006).

Liposome is considered as a spherical vesicle with a permeable wall composed of a lipid bilayer membrane, and the deformation is determined as a function of in-plane shear modulus, H, in combination with out-of-plane bending modulus, B. A dimensionless parameter, $C = a^2H/B$ was introduced for the combined effects of in-plane shear (H) and out-of-plane

bending (B) when a single red blood cell under specific loading configurations (Parker and Winlove1999).

Similar to the equation (3.1), the liposome model was developed based on the large strain formula and can be expressed as

$$T_s^* = T^* + C\left(\frac{1}{\lambda^2} - \lambda^2\right), \tag{4.1}$$

$$T_\theta^* = T^* - C\left(\frac{1}{\lambda^2} - \lambda^2\right), \tag{4.2}$$

where T_s^*, T_θ^* are non-dimensional resultant tensile forces across the membrane thickness in any infinitesimal element, and λ is principal stretch. The non-dimensional- _parameter, ~~The~~ ~~v~~ $C = R_0^2 H / B$, express the relative strengths of the in-plane shear modulus H (N/m) and out-of-plane bending modulus B (Nm) for a liposome of original radius R_o. This important parameter governs the deformed geometric shape of liposome and cell membranes.

The models have been demonstrated to be able simulate the cell deformation under various external loading (Parker and Winlove, 1999, Foo et al 2006). An example of the applications is to simulate the deformation of a bead-attached erythrocyte cell stretched by a point force F at the equator; its detailed experimental is described in Section 5.2 (see Fig 10(b)) (Li et al 2008). For such a case, three governing equations were developed to describe geometric relationships (s~~S~~ee Fig.~~gure~~ 8(a)) as shown in the following

$$\frac{dR}{ds} = \frac{\cos\phi \cdot \sin s}{R}, \tag{4.3}$$

$$\frac{dZ}{ds} = \frac{\sin\phi \cdot \sin s}{R}, \tag{4.4}$$

$$\frac{d\phi}{ds} = \frac{\kappa \cdot \sin s}{R}. \tag{4.5}$$

The other three equations were used to describe balance of bending moment, shearing, and tensile forces as shown below

$$\frac{d\kappa}{ds} = [-Q + \frac{\sin\phi\cos\phi}{R^2} - \frac{\kappa\cos\phi}{R}] \cdot \frac{\sin s}{R} \tag{4.6}$$

$$\frac{dQ}{ds} = [P - (T + \frac{C \cdot \sin s}{R})\kappa - (T + \frac{C \cdot R}{\sin s})\frac{\sin\phi}{R} - \frac{Q \cdot \cos\phi}{R}] \cdot \frac{\sin s}{R}, \tag{4.7}$$

$$\frac{dT}{ds} = \left[C\left(\frac{R}{\sin s} - \frac{\sin s}{R}\right)\frac{\cos\phi}{R} + \kappa Q\right] \cdot \frac{\sin s}{R} - \frac{C \cdot \cos s}{R} + \frac{C \cdot \cos\phi \cdot \sin^2 s}{R^3}. \tag{4.8}$$

If the deformation is assumed to be axisymmetric, the basic boundary conditions are

$$\phi\left(\frac{\pi}{2}\right)=\frac{\pi}{2}, \tag{4.9}$$

$$Q\left(\frac{\pi}{2}\right)=0. \tag{4.10}$$

The simulated deformation of a liposome stretched by applied force *F* for various *C* ranging 0-10, shown as Fig. 8(b)-(d). It is envisaged this mechanical model has a great potential for integration with fluid mechanical model for cell-flow interaction simulation.

4.2 Elastic solid model

AFM indentation was used to measure turgor pressure and surface properties of a single biological cell (Arnoldi et al 2000, Yao et al 2002), and the elasticity of cell membranes (Radmacher et al 1996); the experimental is mentioned in Section 5.1. Recently the technique has been applied to characterize elastic modulus of lipid encapsulated microbubble (Abou-Saleh 2013). Elastic mechanical models, though contradictory sometimes to viscoelastic models, were developed to estimate the materials properties. Among these, Hertz contact model is the most prevailing to analyze the force-displacement curves acquired by indentation experiments. Briefly, when a cell is indented by a spherical probe, the force *F* applied on the cell can be described as function of indentation depth δ as follows,

$$F=\frac{E}{1-\nu^2}\left[\frac{a^2+R_S{}^2}{2}\ln\frac{R_S+a}{R_S-a}-aR_S\right] \tag{4.11}$$

$$\delta=\frac{a}{2}\ln\frac{R_S+a}{R_S-a} \tag{4.12}$$

where *E* and *v* are the Young's Modulus and Poisson's ratio of the cell respectively, α is the radius of indenter-cell contact area, and R_S is the radius of the spherical tip. The Hertz model is only valid for indentations up to 10% of the sample height, substrate effects are considered negligible (Siamantouras et al., 2014).

4.3 Viscoelatic solid model

Having taken into account visco-elasticity of biological cell, Darling *et al* (2006) have developed a simple model which a standard linear solid was integrated with the Hertz equation for modelling small deformation of an isotropic, incompressible solid sphere indented by a hard spherical indenter. The model has been used to characterize the visco-elastic properties of zonal articular chondrocytes. The concise form of the final constitutive relation of the cell is given by

$$F(t)=\frac{4R^{1/2}\delta^{2/3}E_R}{3(1-\nu)}\left(1+\frac{\tau_\sigma-\tau_\varepsilon}{\tau_\varepsilon}e^{-t/\tau_\varepsilon}\right), \tag{4.13}$$

where $F(t)$ is the time-dependent indentation force, δ is the indentation depth, E_R is the relaxation elastic modulus, τ_σ and τ_ε are the relaxation times under constant load and constant strain, respectively.

Roca-Cusachs *et al* (2006) have developed an alternative viscoelastic model for AFM-indentation of cells. They developed force-displacement relationships based on Kelvin viscoelastic model body is:

$$F=\frac{4E_i}{3(1-\nu^2)}R^{1/2}\delta^{3/2}+\frac{2T}{r_t}\pi\delta R, \tag{4.14}$$

where E_i is the Young's modulus of the interior of the cell, T is cortical tension, and r_t is the radius of the AFM tip. Viscoelasticity is then incorporated into the model through converting the shear modulus $G=E/2(1+\nu)$ into the frequency domain as

$$G^*_{NM}(\omega)=G^*_i(\omega)+\kappa_T, \tag{4.15}$$

with

$$\kappa_T=\frac{\pi(1-\nu)}{2r_t}\left(\frac{R}{\delta_0}\right)^{1/2}T, \tag{4.16}$$

$$G^*_i(\omega)=\frac{1-\nu}{4R^{1/2}\delta_o^{1/2}}\left(\frac{F(\omega)}{\delta(\omega)}-i\omega b(0)\right), \tag{4.17}$$

where f is the angular frequency, δ_o is approximate depth around an indentation point, $i\omega b(0)$ is the correction for the viscous drag force exerted by the liquid medium on the AFM cantilever.

5. Experimental techniques

Properties of the coatings of microbubbles, such as their thickness and elasticity, vary significantly among various types of UCAs. For example, lipid coatings (e.g., Sonovue®, Definity®) have a typical thickness of 1-5 nm, thin-shelled protein contrast agents (e.g., Albunex®) have a shell thickness of about 15 nm, while some thick-shelled protein and polymer bubbles (e.g., Quantison™) have coatings 200-300 nm in thickness.

The elastic modulus and viscosity of the encapsulating shell material are two critical parameters for the response of UCAs or liposome subject to ultrasound and ultimately dictate their biomedical performance. Conventional acoustic technique has been long applied to measure scattering and attenuation of ultrasound field passing a suspension solution of

echogenic micro-bubble or liposome (Sarkar et al 2005, Kopechek et al 2011). The viscoelastic properties of the vesicles can be therefore determined indirectly through fitting the experimental results with the data predicted by well-known theories such as Church model (Church 1995) or Hoff model (Hoff et al 2000). De Jong and Hoff (1993) obtained values for the shear and elastic moduli of human serum albumin to characterize Albunex® microbubbles. These values also have been used to study the dynamics of Optison® microbubbles (Stride and Saffari, 2003). Using similar methods, Gorce et al. (2000) estimated the stiffness and viscosity of a phospholipid coating of the contrast agent Sonovue® obtaining a shear modulus, G_s, ~122 MPa and shell viscosity, μ_s, ~2.5 Pa·s, while for albumin coatings (e.g., Albunex®), values for the shear modulus and viscosity of 88.8 MPa and 1.77 Pa·s, respectively, have been reported. In contrast, Postema, de Jong and Schmitz (2005) have reported a much lower value of the elastic modulus for Albunex®, Quantison™ and Sonovue® contrast agents (E = 2 MPa, from which assuming Poisson ration of 0.5, one can estimate $G_s = 0.5\,E_s/(1+\nu) \approx 6$ MPa). For an experimental contrast agent with a polymer-coating from Nycomed (mean diameter ~6 μm and shell thickness ~5% of the particle radius), Hoff et al (2000) reported a shear modulus of 10.6 –12.9 MPa and a shell viscosity of 0.39 – 0.49 Pa·s.

Although the acoustic characterization technique allows to measure these mechanical properties, challenges in experimental setups remain in the attempts to directly measure applied force and corresponding deformation for a single micro-bubble or liposome for accurate determination of its membrane elastic module and viscosity. Typical mechanical forces acting on a single bubble or liposome range from hundreds pico-Newtons (pN) to hundreds micro-Newtons (μm). It is therefore necessary to develop appropriate ultra-sensitive force-displacement measurement instruments for empirical studies. Thanks to the recent advancements in micro-/nano-mechanical force sensing devices, tremendous improvements were made by a spectrum of instruments. These techniques include micropipette technique (Boudou et al 2006), optical tweezers (OT) (Zhang and Liu, 2008), Atomic Force Microscope (AFM) (Abou-Saleh *et al*, 2013), and micro-compression technique (Liu et al 1996). Among these, AFM and OT are the most accurate and prevailing techniques. The former is due to its excellent capabilities of the simultaneous measurements in both deformation and applied force, while the latter owing to its non-contact and cell friendly nature. Other popular methods include compression method which has various formats in terms of its instrumentation such as micro-manipulation method and so-called “cell-poking” technique

(Daily et al 1984), micropipette aspiration method (Simson et al 1999), and magnetic tweezers (Bausch et al 1999) etc.

5.1 Atomic Force Microscopy

The AFM mainly comprises of an ultrasensitive cantilever attached with a probe at its end and a laser beam reflected to a photodetector by the deflection position of the end of the cantilever for measuring the probe-surface interaction (Figure 9). AFM is capable of applying compressive force via the probe to indent a single cell or coated bubble so that the materials parameters can be determined based on the analyses of the force-displacement curves obtained during the cell deformation (Vinckier and Semenza, 1999). Latest advances in life sciences and biomimetics have put the AFM indentation technique in the central stage to investigate biomechanics of both biological and artificial cellular entities. Many single cell mechanics studies were reported using this technique in the past decade due to its ultra-sensitive capability (*ca* 1 pN in force resolution) and wide force range (5 pN to 10000) (Vinckier and Semenza, 1999) For instances, Abou-Saleh *et al* (2013) used AFM to compress lipid encapsulated microbubbles to a large deformation (50%) for both uncoated bubbles and coated with protein coat (streptavidin) or the addition of quantum dots (Q-dots) for determination of their mechanical properties. Chen et al (2013) have applied AFM to study stiffness of phospholipid-coated microbubbles and found the stiffness decreasing exponentially with the microbubble size; thus the finding provided useful insights into cavitation-induced drug delivery. Mahalingam et al (2014) study the compression stiffness of the of Bovine Serum Albumin Stabilized microbubble through AFM nanoindentation and found that the stiffness of the microbubbles increased with the increase of the concentration of BSA solution.

5.2 Optical Tweezers (OT)

Optical Tweezers is a technique to apply non-contact mechanical force to trap particle by using the radiation pressure which is originated from electromagnetic field (Figure 10 (a)). From microscopic point of view, the trapping force is created by the momentum change of photons through a medium or lens. A focused laser beam hitting the particles with a comparatively higher refractive index than the surrounding medium is able to generate a trapping force ranging from 0.1 to 100 pN (Zhang & Liu 2008). The technique has several unique advantages including non-contact, cell-friendly and ultra-high force resolution for studying single cell mechanics (Grier 2003). More importantly, OT is able to manipulate cell within liquid medium which makes it to be the most suitable technique to study cellular mechanical behaviors in cavitation flow (Waleed et al, 2013). Recently optical tweezers have

emerged as a novel tool for manipulating single biological cells and performing sophisticated biomechanical characterizations such as studying the mechanics of a single liposome (Foo et al 2004) as well as characterizing the mechanical properties of single biological cells (Dao et al 2003). Normally two diametrically opposed silica beads (a few micro-meters in diameter) are attached on the cell surface as "handles", through which optical trap force can be applied to deform the cell (Figure 10(b)). Combined with appropriate mechanical models (e.g. elastic shell model described in the section 4.1), the mechanical properties of the cell can be determined based on the degree of cell deformation versus the applied trapped force. For biological cell trapping, the wavelength of 1064nm is often chosen to minimize the absorption by water and cytoskeleton and to avoid possible thermal damage of the trapped cells. Recently, optical tweezers have also been applied to study the mechanics of microbubble. For example, Garbin et al (2007) used optical tweezers combined with ultrahigh speed camera to study the burst and oscillation of a microbubble subject to ultrasonic stimulation and how the interface and neighbouring bubbles influencing on its dynamics behaviours. Jones et al (2006) used scanning optical tweezers to trap ultrasound contrast agent microbubble and measured the transverse drag force which has been found decreasing significantly at small trap radii.

5.3 Compression method

Compression method is to press against a single cell between two parallel plates deforming it into two planar contact circles with the substrates and a torus surface. This method has been applied for a wide spectrum of biological cells. Cole (1932) applied known compressive mechanical forces to deform sea-urchin egg cells and the tensile stress of cell membrane is thus determined based on the subsequent deformed geometry. Adopting a similar compression technique, Zhang *et al.* (1992) developed a micromanipulation technique to press single cells and measured simultaneously the applied force and the sample deformed geometry. The tension modulus and bursting strength were determined using the technique combined with a simple mathematical model. The main challenge in using the parallel plate compression device requiring a high precision positioning of the plate movement is difficult to achieve. Besides, there is no experimental technique which allows continuous measurement of force-displacement curve for the cell during loading/unloading deformation cycles. Later Liu *et al* (1996) developed a micro-compression instrument which employed an ultra-precision micro-stepping motor and force transducer to achieve the continuous compliance measurement of a single cellular entity under compressive deformation. The in-

situ deformation of the cell sample and its instant equatorial diameter was also visualized by a CCD-enhanced microscope system (see Figure 11). The instrument has an ultimate resolution of the force and displacement as 10 nN and 10nm respectively. The technique has been applied to measure the membrane mechanical properties of both biological and non-biological vesicles (e.g. microcapsule) (*Liu* 2006).

5.4 Nano-indentation Method

Daily *et al.* (1984) and Zahalak *et al.* (1990) developed a cell indentation method which involves indenting biological cells with a micro-radius tip (*ca* 2 μm) to measure the loading-unloading responses. In principle, this indentation technique is an extension of the compliance method. There are several possible drawbacks of the method when applying to a cell that comprises of a thin lipid bilayer encapsulating an aqueous content (e.g. cytoplasm). Firstly, indentation provides useful localized mechanical properties only if the indent dimension is small compared to the size of the sample cell at least by a factor of ten, such that the sample resembles a continuum half space. This requirement seems to be violated in the reported experiments by Daily *et al.* (1984) and Zahalak *et al.* (1990). Furthermore, it is an established fact in the literature that when the indentation depth exceeds 10% of the surface film thickness, deformation of the film substrate may be no longer negligible, let alone the inevitable membrane stretching. Such intractable problem further exacerbates in case of small cells where the sample volume remains virtually constant even upon an external load. More importantly, –the observed deformation characteristics can be a very strong but unknown function of the precise geometry of the indenter. These factors present a degree of difficulties in the analysis of measured data for determination of materials parameter.

6. Perspectives

We review an interdisciplinary technique that includes biomechanical testing techniques to determine mechanical properties of single coated micro-bubble and a theoretical model incorporated with the determined parameters to simulate the bubble dynamics. The deformation of bubble coating membrane can be modelled based on Mooney's hyper-elastic constitutive law. However, cell mechanical model may be applied for better describing the lipid membrane of liposome and cell. This technique has important perspectives in studying the following phenomena: (i) the breaking of the bubble coating in releasing drug/gene, (ii) the resultant alteration of cell porosity and permeability, (iii) the role of deformation and

jetting from coated bubbles, (vi) non-spherical shape oscillation of coated bubbles at various mode numbers, and (v) microstreaming around cells due to microbubble oscillation. These fundamental mechanisms remain elusive, are all associated with nonspherical effects and therefore can be expected to be captured only by models using nonspherical bubble dynamics in combination with cell mechanics. The effects of different bubble sizes and location, coatings and membranes (thickness and material) and wave parameters (frequency, wavelength, amplitude and profile) shall be thoroughly studied to access the optimum properties for the drug delivery and sonoporation.

References

Abou-Saleh, R. H., Peyman S. A., Critchley, K., Evans, S. D., & Thomson, N. H. 2013 Nanomechanics of lipid encapsulated microbubbles with functional coatings. *Langmuir* **29**(12), 4096-4103. (DOI: 10.1021/la304093t.)

Arnoldi, M., Fritz, M., Baeuerlein E., Radmacher M., Sackmann, E. & Boulbitch A. 2000 Bacterial turgor pressure can be measured by atomic force microscopy., *Physical Review E*, **62**(1), 1034-1044. (DOI: http://dx.doi.org/10.1103/PhysRevE.62.1034.)

Barthes-Biesel, D. 2003 Flow induced capsule deformation, *Modeling and Simulation of Capsules and Biological Cells*, Edited by C . Pozrikidis, Chapman and Hall/CRC, 1-30.

Bausch A. R., Möller W., & Sackmann E. 1999 Measurement of local viscoelasticity and forces in living cells by magnetic tweezers. *Biophysical Journal*, **76**(1), 573-579. (DOI: 10.1016/S0006-3495(99)77225-5.)

Blake, J. R., Taib, B. B., & Doherty, G. 1986 Transient cavities near boundaries. Part 1. Rigid boundary.*J. Fluid Mech*. **170**,479-497.(DOI: http://dx.doi.org/10.1017/S0022112086000988.)

Blake, J. R., Taib, B. B., & Doherty, G. 1987 Transient cavities near boundaries. Part 2. Free surface. *J. Fluid Mech*. **181**, 197-212. (DOI: http://dx.doi.org/10.1017/S0022112087002052).

Boulton-Stone, J. M., & Blake, J. R. 1993 Gas bubbles bursting at a free surface. *J. Fluid Mech*. **254**, 437-466. (DOI: http://dx.doi.org/10.1017/S0022112093002216.)

Brujan, E. A., Keen, G. S., Vogel, A., & Blake, J. R. 2002 The final stage of the collapse of a cavitation bubble close to a rigid boundary. *Phys. of Fluids*, **14** (1), 85-92, (DOI: http://dx.doi.org/10.1063/1.1421102)

Carson, A. R., McTiernan, C. F., Lavery, L., Hodnick, A., Grata, M., Leng, X., Wang, J. Chen, X., Modzelewski, R. A. & Villanueva, F. S. 2011 Gene therapy of carcinoma using ultrasound-targeted microbubble destruction. *Ultrasound in medicine & biology*, **37**(3), 393-402. (DOI: 10.1016/j.ultrasmedbio.2010.11.011.)

Chen, C. C., Wu, S. Y., Finan, J. D., Morrison III, B., & Konofagou, E. E. 2013 An experimental study on the stiffness of size-isolated microbubbles using atomic force microscopy. *Ultrasonics, Ferroelectrics and Frequency Control, IEEE Transactions on*, **60**(3), 524-534. (DOI:10.1109/TUFFC.2013.2594.)

Chen, H., Kreider, W., Brayman, A. A., Bailey, M. R., & Matula, T. J. 2011 Blood vessel deformations on microsecond time scales by ultrasonic cavitation. *Physical review letters*, **106**(3), 034301. (DOI: http://dx.doi.org/10.1103/PhysRevLett.106.034301)

Church, C.C. 1995 The effects of an elastic solid surface layer on the radial pulsations of gas bubbles *J. Acoust. Soc. Am.* **97**(3), 1510–1521. (http://dx.doi.org/10.1121/1.412091)

Coussios, C. C., Roy, R. A. 2008 Applications of Acoustics and Cavitation to Noninvasive Therapy and Drug Delivery, *Annual Review of Fluid Mechanics*, **40**(1), 395-420. (DOI: 10.1146/annurev.fluid.40.111406.102116)

Curtiss, G. A., Leppinen, D. M., Wang, Q. X. & Blake, J. R. 2013 Ultrasonic cavitation near a tissue layer. *J. Fluid Mech*. **730**, 245-272. (DOI: http://dx.doi.org/10.1017/jfm.2013.341)

Daily, B. I. L. L., Elson, E. L., & Zahalak, G. I. 1984 Cell poking. Determination of the elastic area compressibility modulus of the erythrocyte membrane. *Biophysical journal*, **45**(4), 671-682. (DOI: 10.1016/S0006-3495(84)84209-5)

Darling, E. M., Zauscher, S., & Guilak, F. 2006 Viscoelastic properties of zonal articular chondrocytes measured by atomic force microscopy.*Osteoarthritis and cartilage*, **14**(6), 571-579. (DOI: 10.1016/j.joca.2005.12.003)

Dao, M., Lim, C. T., & Suresh, S. 2003 Mechanics of the human red blood cell deformed by optical tweezers. *Journal of the Mechanics and Physics of Solids*, **51**(11), 2259-2280. (DOI: 10.1016/j.jmps.2003.09.019)

Doinikov, A. A., Haac, J. F., & Dayton, P. A. 2009, Modeling of nonlinear viscous stress in encapsulating shells of lipid-coated contrast agent microbubbles. *Ultrasonics* **49**(2), 269–275. (DOI: 10.1016/j.ultras.2008.09.007.)

Ferrara, K., Pollard, R., & Borden, M. 2007 Ultrasound microbubble contrast agents: fundamentals and application to gene and drug delivery. *Ann. Rev. of Biomed. Eng*., **9**, 415-447. (DOI: 10.1146/annurev.bioeng.8.061505.095852)

Foo, J. J., Liu, K. K., & Chan, V. 2004 Viscous drag of deformed vesicles in optical trap: experiments and simulations. *AIChE journal*, **50**(1), 249-254. (DOI: 10.1002/aic.10023)

Foo, J. J., Chan, V..and Liu, K. K., 2006, Coupling bending and shear effects on liposome deformation, *Journal of Biomechanics*, 39, pp 2338-2343

Gorce, J. M., Arditi, M., & Schneider, M. 2000 Influence of bubble size distribution on the echogenicity of ultrasound contrast agents: a study of Sonovue™. *Investigative radiology*, **35**(11), 661-671.

Grier, D. G. 2003 A revolution in optical manipulation. *Nature*, **424**(6950), 810-816. (doi:10.1038/nature01935)

Garbin, V., Cojoc, D., Ferrari, E., Di Fabrizio, E., Overvelde, M. L. J., Van Der Meer, S. M., De Jong, N., Lohse, D. & Versluis, M. 2007 Changes in microbubble dynamics near a boundary revealed by combined optical micromanipulation and high-speed imaging. *Applied Physics Letters*, **90**(11), 114103. (http://dx.doi.org/10.1063/1.2713164)

Lucca, G., & Prosperetti, A. 1982 A numerical method for the dynamics of non-spherical cavitation bubbles. *In 2d International Colloquium on Drops and Bubbles* **1**, 175-181.

Hsiao, C. T. and Chahine, G. L. 2013 Breakup of finite thickness viscous shell microbubbles by ultrasound: A simplified zero-thickness shell model. J. Acoust. Soc. Am., **133**(4), 1897-1910. (doi: 10.1121/1.4792492)

Hoff, L., Sontum, P. C., & Hovem, J. M. 2000 Oscillations of polymeric microbubbles: Effect of the encapsulating shell. *The Journal of the Acoustical Society of America*, **107**(4), 2272-2280. (http://dx.doi.org/10.1121/1.428557)

Hua, J., & Lou, J. 2007 Numerical simulation of bubble rising in viscous liquid. *Journal of Computational* Physics, 222(2), 769-795. (DOI: 10.1016/j.jcp.2006.08.008)

Ibsen, S., Schutt, C. E., & Esener, S. 2013 Microbubble-mediated ultrasound therapy: a review of its potential in cancer treatment. *Drug design, development and therapy*, **7**, 375–388.(doi: 10.2147/DDDT.S31564)

Jayaprakash, A., Singh, S., & Chahine, G. 2011 Experimental and numerical investigation of single bubble dynamics in a two-phase bubbly medium. *Journal of Fluids Engineering*, **133**(12), 121305. (doi:10.1115/1.4005424)

Johnsen, E., & Colonius, T. 2008 Shock-induced collapse of a gas bubble in shockwave lithotripsy. *The Journal of the Acoustical Society of America*, **124**(4), 2011-2020. (http://dx.doi.org/10.1121/1.2973229)

Johnsen, E., & Colonius, T. 2009 Numerical simulations of non-spherical bubble collapse. *J. Fluid Mech.*,**629**,231-262. (DOI: http://dx.doi.org/10.1017/S0022112009006351)

Jones, P. H., Stride, E., & Saffari, N. 2006 Trapping and manipulation of microscopic bubbles with a scanning optical tweezer. *Appl. Phys. Lett*, **89**(8), 081113. (http://dx.doi.org/10.1063/1.2338512)

de Jong, N., & Hoff, L. 1993 Ultrasound scattering properties of Albunex microspheres. *Ultrasonics*, **31**(3), 175-181. (DOI: 10.1016/0041-624X(93)90004-J)

Kaul, S. 2004 Microbubbles and ultrasound: a bird's eye view. Trans. *Am. Clin. Climatol. Assoc.*, **115**, 137-148. (PMCID: PMC2263759)

Klaseboer, E., Fong, S. W., Turangan, C. K., Khoo, B. C., Szeri, A. J., Calvisi, M. L., Sankin, G. N. and Zhong, P. 2007 Interaction of lithotripter shockwaves with single inertial cavitation bubbles. *J. Fluid Mech*. **593**, 33–56. (DOI: http://dx.doi.org/10.1017/S002211200700852X)

Kopechek J. A., Haworth K. J., Raymond J. L., Mast, T. D., Perrin Jr S. R., Klegerman, M. E., Huang, S., Porter T. M., McPherson D. D., Holland C. K. 2011). Acoustic characterization of echogenic liposomes: Frequency-dependent attenuation and backscatter. *J. Acoust. Soc. Am*. **130**(5):3472-3481. (http://dx.doi.org/10.1121/1.3626124)

Lauterborn, W., & Kurz, T. 2010 Physics of bubble oscillations. *Reports on Progress in Physics*, **73**(10), 106501. (doi:10.1088/0034-4885/73/10/106501)

Li, C., Liu, Y. P., Liu, K. K., & Lai, A. C. 2008 Correlations between the experimental and numerical investigations on the mechanical properties of erythrocyte by laser stretching. *NanoBioscience, IEEE Transactions on*, **7**(1), 80-90. (DOI: 10.1109/TNB.2008.2000152)

Lind, S. J., & Phillips, T. N. 2012 The influence of viscoelasticity on the collapse of cavitation bubbles near a rigid boundary. *Theor. Comput. Fluid Dyn.*, **26**(1-4), 245-277. (DOI: 10.1007/s00162-011-0227-9)

Liu, K. K., Williams, D. R., & Briscoe, B. J. 1996 Compressive deformation of a single microcapsule. *Phy. Rev. E*, **54**(6), 6673-6680. (DOI: http://dx.doi.org/10.1103/PhysRevE.54.6673)

Liu K. K., 2006, Deformation behaviours of soft particles – a review, *J. Phys. D: Appl. Phys*., 39, pp R189-R199

Liu, Y. P., Li, C., Liu, K. K., & Lai, A. C. 2006 The deformation of an erythrocyte under the radiation pressure by optical stretch. *Journal of biomechanical engineering*, **128**(6), 830-836. (doi:10.1115/1.2354204)

Liu, Y., Sugiyama, K., Takagi, S., & Matsumoto, Y. 2012 Surface instability of an encapsulated bubble induced by an ultrasonic pressure wave. *J. Fluid Mech.*, **691**, 315-340. (DOI: http://dx.doi.org/10.1017/jfm.2011.477)

Lundgren, T. S., & Mansour, N. N. 1988 Oscillations of drops in zero gravity with weak viscous effects. . *J. Fluid Mech.*, **194**, 479-510. (DOI: http://dx.doi.org/10.1017/S0022112088003076)

Mahalingam, S., Meinders, M. B., & Edirisinghe, M. J. 2014 The formation, stability, and mechanical properties of bovine serum albumin stabilised air bubbles produced using co-axial electrohydrodynamic atomisation. *Langmuir*, **30**(23), 6694−6703. (DOI: 10.1021/la5011715)

Marmottant, P., & Hilgenfeldt, S. 2003 Controlled vesicle deformation and lysis by single oscillating bubbles. *Nature*, **423**(6936), 153-156.

Pamplona, D. C., & Calladine, C. R. 1993 The mechanics of axially symmetric liposomes. *J. Biom. Eng.-Transaction of the ASME*, **115**(2), 149-159. (doi:10.1115/1.2894115)

Paul, S., Nahire, R., Mallik, S., & Sarkar, K. 2014 Encapsulated microbubbles and echogenic liposomes for contrast ultrasound imaging and targeted drug delivery. *Computational Mechanics*, **53**(3), 413-435. (DOI:10.1007/s00466-013-0962-4)

Postema, M., de Jong, N., & Schmitz, G. 2005 The physics of nanoshelled microbubbles. Biomed. Tech, **50**(S1), 748-749.

Radmacher, M., Fritz, M., Kacher, C. M., Cleveland, J. P., & Hansma, P. K. 1996 Measuring the viscoelastic properties of human platelets with the atomic force microscope. *Biophysical journal*, **70**(1), 556-567. (DOI: 10.1016/S0006-3495(96)79602-9)

Roca-Cusachs, P., Almendros, I., Sunyer, R., Gavara, N., Farré, R., & Navajas, D. 2006 Rheology of passive and adhesion-activated neutrophils probed by atomic force microscopy. *Biophysical journal*, **91**(9), 3508-3518. (DOI: 10.1529/biophysj.106.088831)

J. Rodr´ıguez-Rodr´ıguez, A. Sevilla,C. Mart´ınez-Baz´an,2 and J.M. Gordillo 2015 Generation of Microbubbles with Applications to Industry and Medicine. Annual Review of Fluid Mechanics 47: 405-429 (DOI: 10.1146/annurev-fluid-010814-014658)

Sarkar, K., Shi, W. T., Chatterjee, D., & Forsberg, F. 2005 Characterization of ultrasound contrast microbubbles using in vitro experiments and viscous and viscoelastic interface models for encapsulation. *J. Acoust. Soc. Am.*, **118**(1), 539-550. (http://dx.doi.org/10.1121/1.1923367)

Schroeder, A., Kost, J., & Barenholz, Y. 2009 Ultrasound, liposomes, and drug delivery: principles for using ultrasound to control the release of drugs from liposomes. *Chemistry and physics of lipids*, **162**(1), 1-16. (DOI: 10.1016/j.chemphyslip.2009.08.003)

Sirsi, S. R., & Borden, M. A. 2009 Microbubble compositions, properties and biomedical applications. *Bubble Science, Engineering & Technology*, **1**(1-2), 3-17. (DOI: http://dx.doi.org/10.1179/175889709X446507)

Simson, D. A., Ziemann, F., Strigl, M., & Merkel, R. 1998 Micropipet-based pico force transducer: in depth analysis and experimental verification. *Biophysical journal*, **74**(4), 2080-2088. (DOI: 10.1016/S0006-3495(98)77915-9)

Skalak, R., Tozeren, A., Zarda, R. P., & Chien, S. 1973 Strain energy function of red blood cell membranes. *Biophysical Journal*, **13**(3), 245-264. (DOI: 10.1016/S0006-3495(73)85983-1)

Shen, Z. P., Brayman, A. A., Chen, L., & Miao, C. H. 2008 Ultrasound with microbubbles enhances gene expression of plasmid DNA in the liver via intraportal delivery. *Gene therapy*, **15**(16), 1147-1155. (doi:10.1038/gt.2008.51)

Stride, E., & Saffari, N. 2003 Microbubble ultrasound contrast agents: a review. Proceedings of the Institution of Mechanical Engineers, Part H: *J. Eng. Medi*, **217**(6), 429-447. (doi: 10.1243/09544110360729072)

Sundaram, J., Mellein, B. R., & Mitragotri, S. 2003 An experimental and theoretical analysis of ultrasound-induced permeabilization of cell membranes. *Biophysical journal*, **84**(5), 3087-3101. (DOI: 10.1016/S0006-3495(03)70034-4)

Szeri, A. J., Storey, B. D., Pearson, A., & Blake, J. R. 2003 Heat and mass transfer during the violent collapse of nonspherical bubbles. *Phys. Fluids*, **15**(9), 2576-2586. (http://dx.doi.org/10.1063/1.1595647)

Tsigklifis, K., & Pelekasis, N. A. 2013 Simulations of insonated contrast agents: Saturation and transient break-up. *Phys. Fluids*, **25**(3), 032109. (http://dx.doi.org/10.1063/1.2061872)

Tsutsui, J. M., Xie, F., & Porter, R. T. 2004 The use of microbubbles to target drug delivery. *Cardiovasc Ultrasound*, **2**(1), 23. (doi:10.1186/1476-7120-2-23)

Vinckier, A., & Semenza, G. 1998 Measuring elasticity of biological materials by atomic force microscopy. *Febs Letters*, **430**(1), 12-16. (DOI: 10.1016/S0014-5793(98)00592-4)

Waleed, M., Hwang, S. U., Kim, J. D., Shabbir, I., Shin, S. M., & Lee, Y. G. 2013 Single-cell optoporation and transfection using femtosecond laser and optical tweezers. *Biomedical optics express*, **4**(9), 1533-1547. (http://dx.doi.org/10.1364/BOE.4.001533)

Wang, Q. X. 2013 Non-spherical bubble dynamics of underwater explosions in a compressible fluid. *Phys. Fluids*, **25**, 072104. (http://dx.doi.org/10.1063/1.4812659)

Wang, Q. 2014 Multi-oscillations of a bubble in a compressible liquid near a rigid boundary. *J. Fluid Mech.*, **745**, 509-536. (DOI: http://dx.doi.org/10.1017/jfm.2014.105)

Wang, Q. X. & Blake, J. R. 2010 Non-spherical bubble dynamics in a compressible liquid. Part 1. Travelling acoustic wave. *J. Fluid Mech*. **659**, 191-224. (DOI: http://dx.doi.org/10.1017/S0022112010002430)

Wang, Q. X. & Blake J. R. 2011 Non-spherical bubble dynamics in a compressible liquid. Part 2. Acoustic standing wave. *J. Fluid Mech*. **679**, 559-581. (DOI: http://dx.doi.org/10.1017/jfm.2011.149)

Wang, Q. X. 1998 The numerical analyses of the evolution of a gas bubble near an inclined wall. *Theoret. & Comput. Fluid Dyn*. **12**, 29-51.

Wang, Q. X. 2004 Numerical modelling of violent bubble motion. *Phys. Fluids* 16 (5), 1610-1619. (http://dx.doi.org/10.1063/1.1704645)

Wang, Q. X., Yeo, K. S., Khoo, B. C. & Lam, K. Y. 1996a Nonlinear interaction between gas bubble and free surface. *Computers & Fluids* **25** (7), 607-628. (DOI: 10.1016/0045-7930(96)00007-2)

Wang, Q. X., Yeo, K. S., Khoo, B. C. & Lam, K. Y. 1996b Strong interaction between buoyancy bubble and free surface. *Theor . Comput. Fluid Dyn.* **8**(1), 73-88. (DOI:

10.1007/BF00312403)

Wang, Q. X., Yeo, K. S., Khoo, B. C. & Lam, K. Y. 2005 Vortex ring modelling for toroidal bubbles. *Theoret. & Comput. Fluid Dyn.* **19** (5), 303-317. (DOI: 10.1007/s00162-005-0164-6)

Waugh, R. E., Song, J. I. A. N. B. E. N., Svetina, S., & Zeks, B. 1992 Local and nonlocal curvature elasticity in bilayer membranes by tether formation from lecithin vesicles. *Biophysical journal*, **61**(4), 974-982. (DOI: 10.1016/S0006-3495(92)81904-5)

Yao, X., Walter, J., Burke, S., Stewart, S., Jericho, M. H., Pink, D., Hunter R. & Beveridge, T. J. 2002 Atomic force microscopy and theoretical considerations of surface properties and turgor pressures of bacteria. *Colloids and Surfaces B: Biointerfaces*, **23**(2-2), 213-230. (DOI: 10.1016/S0927-7765(01)00249-1)

Yu, H., & Xu, L. 2014 Cell experimental studies on sonoporation: State of the art and remaining problems. *Journal of Controlled Release*, **174**, 151-160. (DOI: 10.1016/j.jconrel.2013.11.010)

Yue, P., Feng, J. J., Bertelo, C. A., & Hu, H. H. 2007 An arbitrary Lagrangian–Eulerian method for simulating bubble growth in polymer foaming. *J. Comput. Phys.*, **226**(2), 2229-2249.(DOI: 10.1016/j.jcp.2007.07.007)

Zahalak, G. I., McConnaughey, W. B., & Elson, E. L. 1990 Determination of cellular mechanical properties by cell poking, with an application to leukocytes. *Journal of biomechanical engineering*, **112**(3), 283-294. (doi:10.1115/1.2891186)

Zhang, H., & Liu, K. K. 2008 Optical tweezers for single cells. *Journal of The Royal Society Interface*, **5**(24), 671-690. (doi: 10.1098/rsif.2008.0052)

Figure Legends

Figure 1. Vascular rupture involving a liquid jet. Amplitude of ultrasound = 4 MPa. Vessel diameter = 15 μm. Sketches of the bubble jet in solid lines and microvessel in dashed lines, adapted from Chen et al (2011).

Figure 2. (a) Structure of liposome, (b) Ultrasonic cavitation induce the drug release from liposome.

Figure 3. Schematic of an encapsulated microbubble subject to ultrasonic wave, travelling near a rigid wall.

Figure 4: Comparisons of the bubble radius time history for a coated and uncoated bubble as determined from the 3D BIM model and modified Rayleigh-Plesset equation (RP). The parameters used for the case are c = 1500 m/s, $\alpha = 1.4$, $\sigma = 0.055$ N/m, $\varepsilon = 1+2\sigma^*$, $p_0 = 100$ kPa, $\rho = 1000$ kg/m^3, $R_0 = 4.5$ μm, $p_{a^*} = 1.2$, $f = 0.3$ MHz, $G_s = 10.0$ MPa, $d_s = 15$ nm, $\mu_s = 0$, and $\mu_L = 3.5$ Pa s (R_e=13).

Figure 5. Coated bubble dynamics near a wall subject to ultrasound propagating parallel to the wall for $\gamma = 3.0$, $p_{a^*} = 2.0$ with the remaining parameters the same as in figure 3. The bubble shapes are shown during the expansion phase (a-b) and collapse phase (b-d).

Figure 6. Coated bubble dynamics near a wall subject to ultrasound propagating parallel to the wall for $\gamma = 2.0$, $p_{a^*} = 2.0$ with the remaining parameters the same as in figure 3. The bubble shapes are shown during the expansion phase (a-b) and collapse phase (b-d).

Figure 7. Coated bubble dynamics near a wall subject to ultrasound propagating parallel to the wall for $\gamma = 1.0$, $p_{a^*} = 2.0$ with the remaining parameters the same as in figure 3. The bubble shapes are shown during the expansion phase (a-b) and collapse phase (b-d).

Figure 8. (a) Cell membrane under deformation described by Liposome model, (b)-(d) The simulated meridional profiles of the cell membrane following deformation in the Z direction, shown for $C = 0 - 10$.

Figure 9 Schematic of AFM to indent a single cell for mechanical characterization.

Figure 10 (a) Schematic of working principle of optical tweezers (OT) (b) using OT to stretching single cell for mechanical characterization

Figure 11 Schematic Diagram of Cell Characterisation Instrument Set-Up (not in scale)

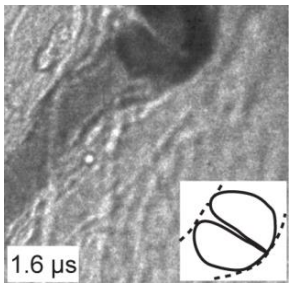

Fig. 1

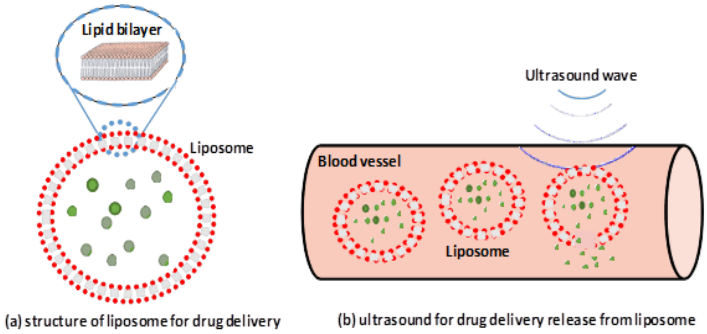
Lipid bilayer
Liposome
(a) structure of liposome for drug delivery
Ultrasound wave
Blood vessel
Liposome
(b) ultrasound for drug delivery release from liposome

Fig. 2

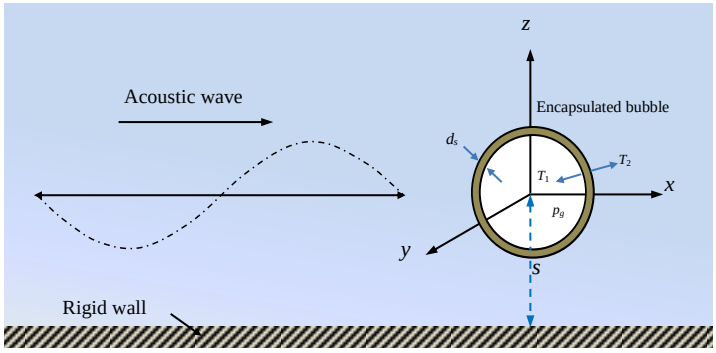
z
Acoustic wave
Encapsulated bubble
d_s
T_1
T_2
x
p_g
y
S
Rigid wall

Fig. 3

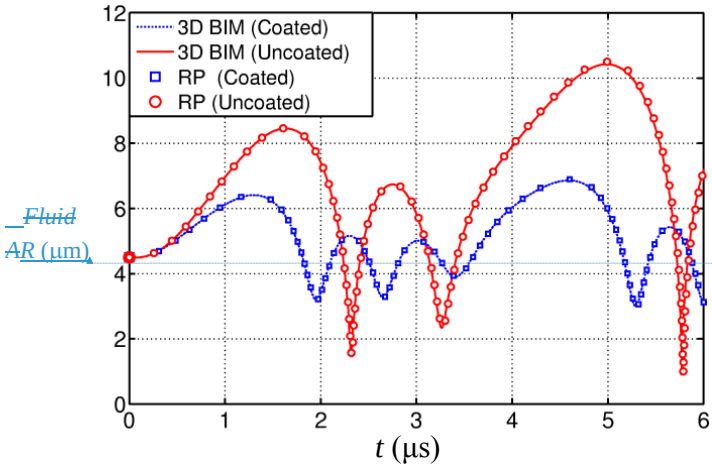

Fluid
AR (μm)

Formatted: Font: 12 pt

Fig. 4

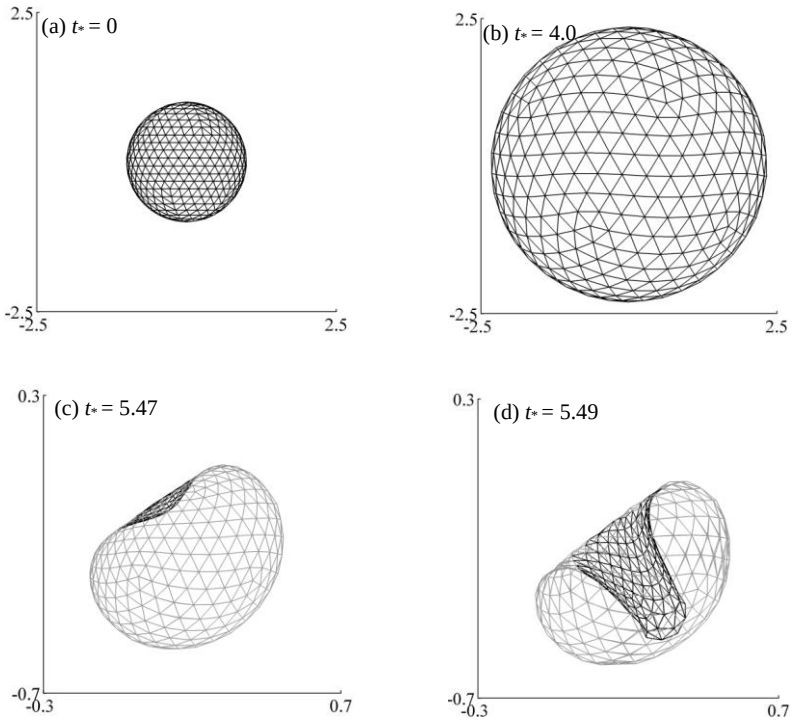

Fig. 5

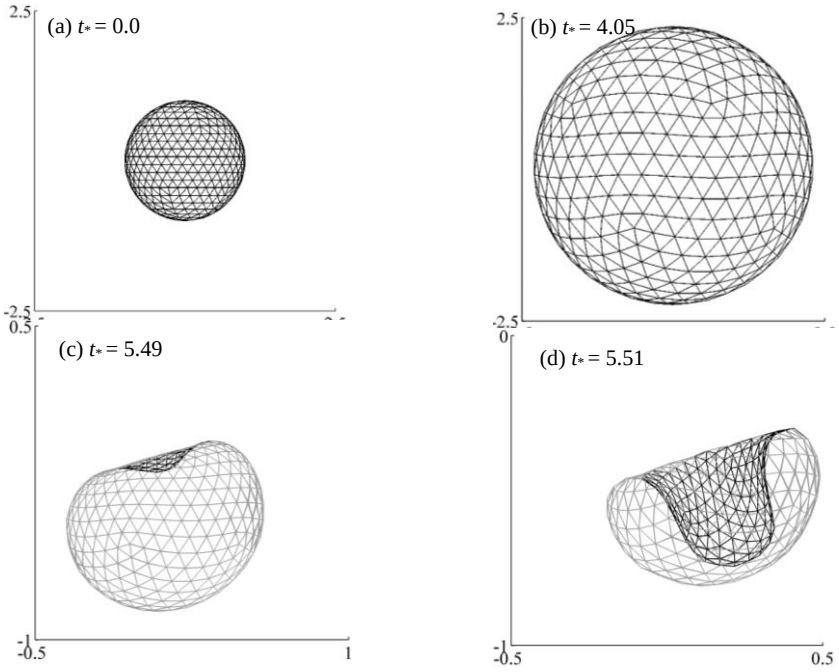

Fig. 6

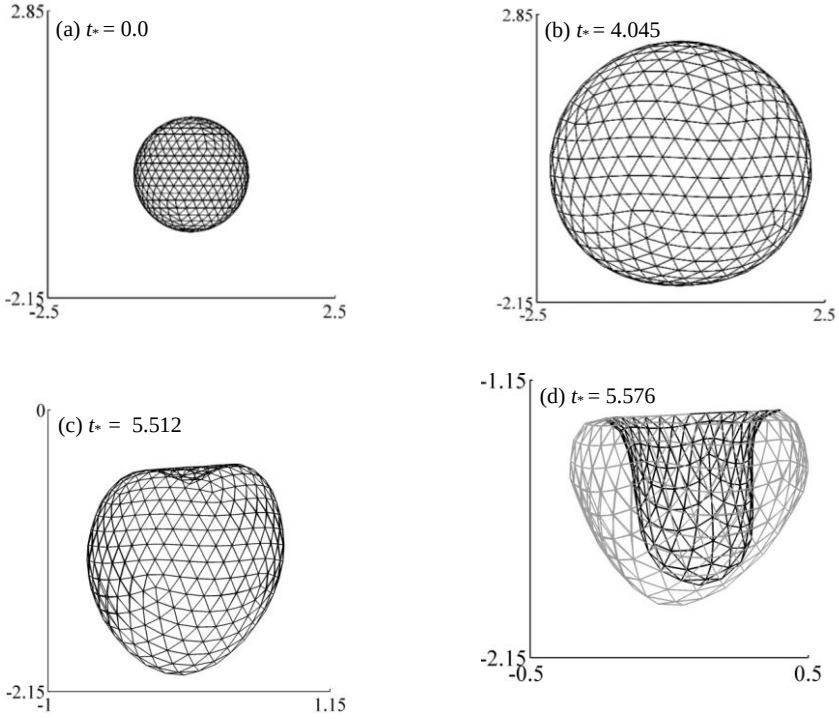
2.85
(a) t_* = 0.0
-2.15
-2.5
2.5
2.85
(b) t_* = 4.045
-2.15
-2.5
2.5
0
(c) t_* = 5.512
-2.15
-1
1.15
-1.15
(d) t_* = 5.576
-2.15
-0.5
0.5

Fig. 7

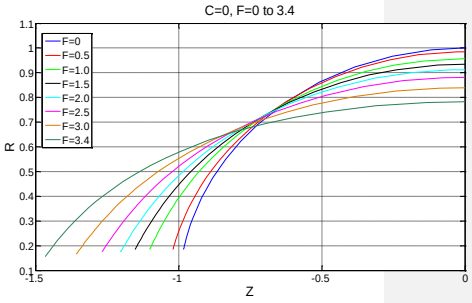
C=0, F=0 to 3.4
F=0
F=0.5
F=1.0
F=1.5
F=2.0
F=2.5
F=3.0
F=3.4
R
Z

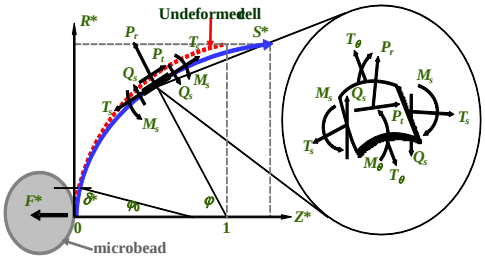
R*
Undeformed cell
S*
F*
δ*
φ0
φ
Z*
0
1
microbead

(a(

~~b~~)

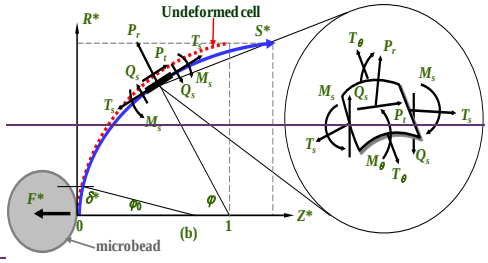
R*
Undeformed cell
S*
F*
δ*
φ0
φ
Z*
0
1
(b)
microbead

(b)

Formatted: Space After: 15 pt

Formatted: Justified, Space After: 15 pt

Fig 8

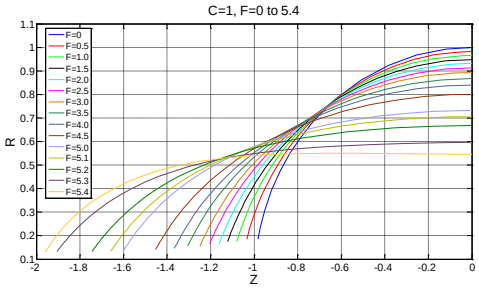

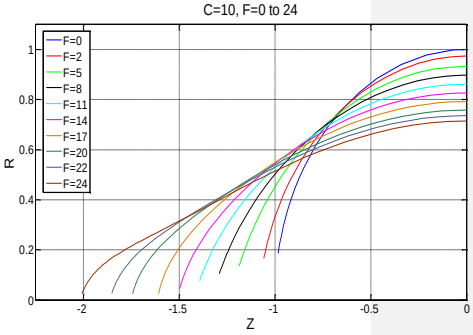

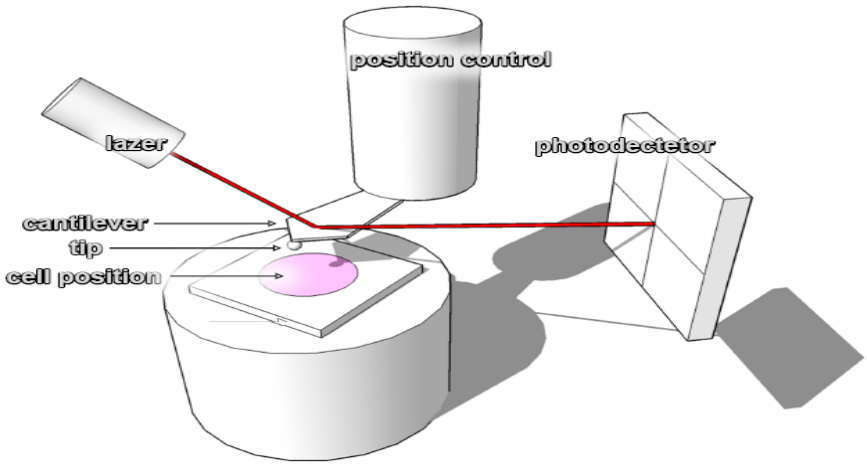
position control
lazer
photodectetor
cantilever
tip
cell position

Fig. 9

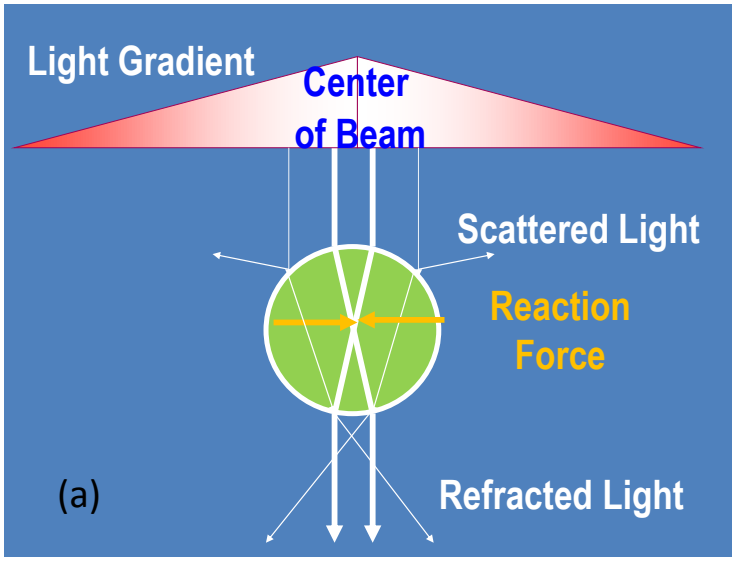
Light Gradient
Center
of Beam
Scattered Light
Reaction
Force
(a)
Refracted Light

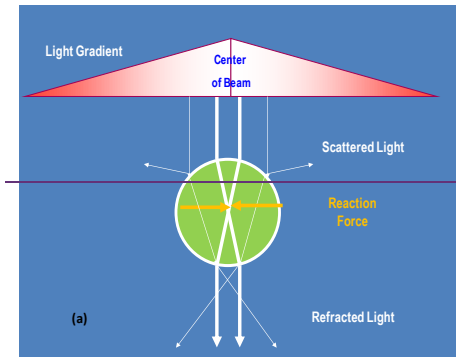
Light Gradient
Center
of Beam
Scattered Light
Reaction
Force
(a)
Refracted Light

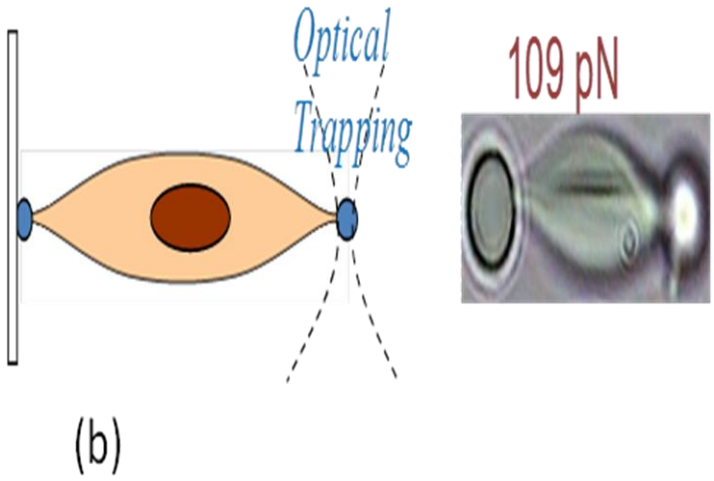
Optical
Trapping
109 pN
(b)

Fig. 10

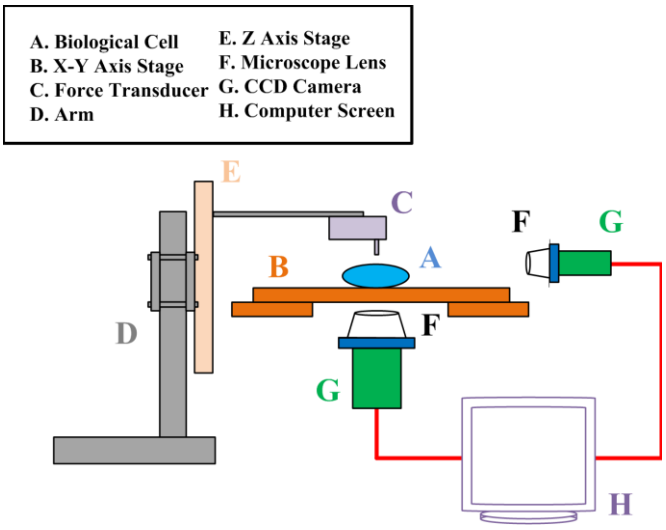
A. Biological Cell
B. X-Y Axis Stage
C. Force Transducer
D. Arm
E. Z Axis Stage
F. Microscope Lens
G. CCD Camera
H. Computer Screen
E
C
F
G
B
A
D
F
G
H

Fig. 11